ARL-TR-8507 • Sep 2018

US Army Research Laboratory

Anisotropic Grain Growth Modeling under the SPPARKS Framework

by Efraín Hernández–Rivera, Philip E Goins, and Heather A Murdoch

NOTICES

Disclaimers

The findings in this report are not to be construed as an official Department of the Army position unless so designated by other authorized documents.

Citation of manufacturer's or trade names does not constitute an official endorsement or approval of the use thereof.

Destroy this report when it is no longer needed. Do not return it to the originator.

ARL-TR-8507 ● SEP 2018

US Army Research Laboratory

Anisotropic Grain Growth Modeling under the SPPARKS Framework

by Efraín Hernández–Rivera and Heather A Murdoch
Weapons and Materials Research Directorate, ARL

Philip E Goins
Oak Ridge Institute for Science and Education, Oak Ridge, TN

REPORT DOCUMENTATION PAGE

Form Approved
OMB No. 0704-0188

1. REPORT DATE *(DD-MM-YYYY)*
September 2018

2. REPORT TYPE
Technical Report

3. DATES COVERED (From - To)
January 2017–January 2018

4. TITLE AND SUBTITLE
Anisotropic Grain Growth Modeling under the SPPARKS Framework

5a. CONTRACT NUMBER

5b. GRANT NUMBER

5c. PROGRAM ELEMENT NUMBER

6. AUTHOR(S)
Efraín Hernández–Rivera, Philip E Goins, and Heather A Murdoch

5d. PROJECT NUMBER

5e. TASK NUMBER

5f. WORK UNIT NUMBER

7. PERFORMING ORGANIZATION NAME(S) AND ADDRESS(ES)
US Army Research Laboratory
ATTN: RDRL-WMM-B
Aberdeen Proving Ground, MD 21005-5066

8. PERFORMING ORGANIZATION REPORT NUMBER
ARL-TR-8507

9. SPONSORING/MONITORING AGENCY NAME(S) AND ADDRESS(ES)

10. SPONSOR/MONITOR'S ACRONYM(S)

11. SPONSOR/MONITOR'S REPORT NUMBER(S)

12. DISTRIBUTION/AVAILABILITY STATEMENT
Approved for public release; distribution is unlimited.

13. SUPPLEMENTARY NOTES
primary author's email: <efrain.hernandez18.civ@mail.mil>.

14. ABSTRACT
The Potts Monte Carlo model is often used simulate parabolic grain growth. The Stochastic Parallel PARticle Kinetic Simulator (SPPARKS) framework is a highly efficient computational tool where the Potts model has been successfully implemented. However, it has only been extended to isotropic systems where each grain feature is defined by a single orientation classifier. A more complete microstructural description can be implemented where each grain orientation is defined by the Euler–Bunge angles. The *AppPottsRS* code (C++ class), where grain are defined through Euler angles, was developed as a SPPARKS compatible application. Based on the Read–Shockley equation, AppPottsRS uses the more robust microstructural description (Euler angles) to define how unlike grains interact (i.e., though a grain boundary energy Hamiltonian). This technical report shows that AppPottsRS captures all of the expected characteristics of ideal grain growth. Further, the importance of detailed analysis of the simulated data is showcased through characterization of curvature-driven and thermally enhanced grain growth simulations.

15. SUBJECT TERMS
Potts Monte Carlo, anisotropic grain growth, misorientation angle, quaternion, Read–Shockley, SPPARKS

16. SECURITY CLASSIFICATION OF:			**17. LIMITATION OF ABSTRACT**	**18. NUMBER OF PAGES**	**19a. NAME OF RESPONSIBLE PERSON**
a. REPORT	**b. ABSTRACT**	**c. THIS PAGE**			Efraín Hernández–Rivera
Unclassified	Unclassified	Unclassified	UU	34	**19b. TELEPHONE NUMBER (Include area code)** 410-306-4961

Contents

List of Figures

List of Tables

1. Introduction

Microstructural features are known to play an important role on materials properties and performance. A fairly well-known example is the Hall–Petch effect where the yield strength depends on the average grain size.[1,2] Furthermore, grain size influences other material properties like corrosion resistance,[3] electrical conductivity,[4,5] and radiation tolerance.[6] Other advanced applications where microstructural features play a critical role include the engineering of refractory high entropy alloys where the resulting microstructures influences their stability.[7] Therefore, understanding of microstructural evolution has become paramount as these advanced manufacturing techniques can enable the materials-by-design paradigm. While analytical models are shown to predict general microstructure evolutionary characteristics (e.g., parabolic grain growth, processing materials under complex constraints requires more complex mesoscale models). Hence, there is a need for computational models that are able to simulate microstructural evolution at mesoscales. Furthermore, these models need to properly account for realistic physics (e.g., anisotropic interfacial interactions), which are known to influence mechanical properties.[8]

Multiple computational techniques have been successfully implemented to simulate microstructural evolution. Some of these computational approaches include level-set,[9] phase field,[10] and the Q-state Monte Carlo[11] methods. The latter, also known as the Potts Monte Carlo (PMC) or Q-state Ising model, has been widely implemented to simulate curvature-driven grain growth with a surprising degree of agreement to material systems following parabolic grain growth. It was initially developed as a generalization to the Ising model[12,13] to model interacting *spins* on a crystalline lattice. Over the last few decades, it has been successfully implemented to study grain growth and texture evolution.[14–17] While it is proven successful in modeling microstructural evolution, its popularity stems from its simplicity to implement and understand. A broader appeal to the mathematics and traditional physics community is that it is exactly solvable when reduced to one dimension.[18] Due to its popularity and simplicity, a variety of codes and implementations have been developed. In order to unify these efforts, the *Stochastic Parallel PARticle Kinetic Simulator* (SPPARKS) framework was developed at Sandia National Laboratories.[19] However, the SPPARKS implementation focuses on isotropic systems and development of efficient algorithms, (e.g., rejection-free Potts Neighbor-Only).[20]

While SPPARKS has enabled the streamlined use of the PMC, its lack of texture information can limit its applicability to a wide range of materials problems. An often-used alternative is to describe interfacial energies by the Read–Shockley (RS) equation, which defines the energy between two neighboring grains that are misoriented by θ to each other. This technical report outlines the development of the RS formulation into SPPARKS as the new C++ *AppPottsRS* class.[21] The SPPARKS framework is leveraged due to its efficiency and multiprocessing implementation. The AppPottsRS implementation is benchmarked to its equivalent Potts Neighbor-Only application and against the well-established literature on ideal grain growth. Lastly, microstructural evolution under thermal gradients is demonstrated.

2. Model Development

The PMC model has been widely used across multiple physics disciplines. This section includes a discussion on how the PMC is generally implemented, and introduces the physics relevant to the AppPottsRS class. This includes definitions for the computational domain (in terms of grain orientations), the kinetics and thermodynamics that govern microstructural evolution, and a brief overview on the RS model.[22]

2.1 Microstructural Representation

As with traditional Monte Carlo models, the PMC model uses a discretized lattice where each discrete element describes a particular feature. For microstructural modeling, these discrete features can represent magnetic domains, phases, and/or grain orientation, *inter alia*. Here, microstructure refers to a grain's orientation with the set of allowable orientations given by

$$Q = \{q_0, \ldots, q_i, \ldots, q_N\} \tag{1}$$

where q_i is the orientation state for the i-th discrete element. A discretized meshless-rectangular Euclidean domain is used as the simulation lattice, shown in Fig. 1. This example *microstructure* comprises a 2-D computational domain with periodic boundaries where each material node (pixel, or voxel in 3-D) can be oriented into six different directions. It should be noted that nonrectangular meshes (e.g., triangular or hexagonal) are regularly used. In this example, the grain orientation is given as an integer (color), but this is not a requirement.

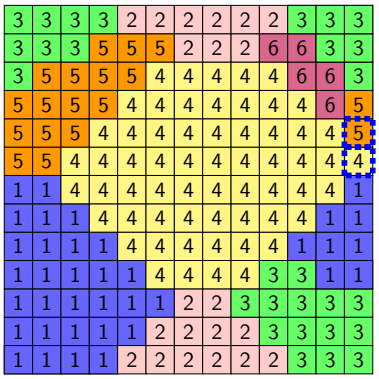

Fig. 1 Schematic of a meshless computational domain typically used for PMC models

An alternative microstructural representation replaces the integer-based orientation with a set of rotation angle as defined by Euler. As AppPottsRS requires information on grain boundary misorientation, each q-state is defined by a set of Euler–Bunge angles

$$q_i = \{\phi_1, \Phi, \phi_2\}_i \tag{2}$$

where these angles define the axial rotation to bring the laboratory axes into concurrence with the crystalline axes. Using these angles, the misorientation angle (θ) between two neighboring grains g_A and g_B can be determined by

$$\theta = \Delta g_{AB} = (O_B^{sym}\mathbf{g}_B) \cdot (O_A^{sym}\mathbf{g}_A)^{-1} \tag{3}$$

where $\mathbf{g}_i$ and O_i^{sym} are the i-th grain's orientation matrix and the material-specific symmetry operator. The symmetry operators reduce the number of unique misorientations required to represent all possible misorientations, which are limited due to the crystal symmetry. AppPottsRS has been developed to include cubic and hexagonal crystal symmetries, which have 24 and 12 symmetrically related orientations, respectively. Hence, when using this microstructural representation, the state for each material node (voxel) will be defined by a set of angles.

Representing the computational domain in terms of Euler–Bunge angles provides a fuller description of the microstructure. However, for many representations of 3-D angular orientation, rotation computation is complex or expensive. Euler angles do not lend themselves to such transformations directly, especially with symmetry operators involved. Further, sets of three orientation angles suffer from so-called gimbal lock, where certain conditions "lock" grain orientations into degenerate spaces

(in the Bunge notation, this occurs when $\Phi = \{0, \pi\}$). In this technical report, orientation and misorientations are computed using quaternions, which are length-4 arrays defined as

$$\mathbf{q} = q_0 + \mathsf{q}_1\mathbf{i} + \mathsf{q}_2\mathbf{j} + \mathsf{q}_3\mathbf{k} \tag{4}$$

where $\mathsf{q}_0, \mathsf{q}_1, \mathsf{q}_2$, and q_3 are the real numbered quaternion coefficients (not to be confused with the $q-$state). These are derived from the Euler angles as

$$\begin{aligned}
\mathsf{q}_0 &= \cos\left(\frac{\Phi}{2}\right)\cos\left(\frac{\phi_1+\phi_2}{2}\right)\\
\mathsf{q}_1 &= \sin\left(\frac{\Phi}{2}\right)\cos\left(\frac{\phi_1-\phi_2}{2}\right)\\
\mathsf{q}_2 &= \sin\left(\frac{\Phi}{2}\right)\sin\left(\frac{\phi_1-\phi_2}{2}\right)\\
\mathsf{q}_3 &= \cos\left(\frac{\Phi}{2}\right)\sin\left(\frac{\phi_1+\phi_2}{2}\right).
\end{aligned} \tag{5}$$

A corresponding operation is applied for matrices in order to represent the symmetry operators in quaternion form (see Hernández–Rivera[21]). The misorientation angle between grains is calculated by taking the Hamilton product between quaternions.

Traditionally, most numerical implementations employ a 3×3 orientation matrix to define the grain orientation and calculate grain boundary misorientation. Compared to matrices, quaternions require less memory (4 values per angle instead of 9 per voxel), are more computationally efficient (16 operations instead of 27 per multiplication step), avoid degeneracy during gimbal lock, offer a very simple extraction of axis-angle values for any given rotation, and are less sensitive to loss of precision due to rounding errors in floating point operation. The primary disadvantage of unit quaternions is that each rotation matrix could be represented by a pair of conjugate quaternions, which requires care and an additional computation step when comparing two rotations.

2.2 Q-State Monte Carlo

Much like the Ising model, the PMC model aims to simulate interactions between "spins" on a lattice. However, the PMC model generalizes spins as a Q-leveled set of states. Under this premise, microstructural evolution is modeled by kinetically limited attempts to update a site's state to an *allowable* state. Each time a trial state is accepted, a grain is said to have grown. The PMC model execution starts by randomly selecting a site and attempting a change from its current spin value q_i to its neighbor's q_j, such as site $q_i = 5 \rightarrow q_i = q_j = 4$ (blue dashed boxes at the right-most column in Fig. 1). If such an event is accepted, the global energy is then reduced. The mathematical formulation defining the energy state, and whether this flip results in an energy decrease, is given by the Hamiltonian

$$\mathcal{H} = \sum_{i=1}^{N} \left[U_i + \frac{1}{2} \sum_{j=1}^{n_{nei}} \gamma_{ij} \left(1 - \delta_{q_i,q_j}\right) \right] \tag{6}$$

where N is the total number of lattice points, n_{nei} is the number of surrounding neighbors, U_i is the bulk (volumetric) energy, γ_{ij} is the interaction strength, and δ_{q_i,q_j} is the Kronecker delta

$$\delta_{q_i,q_j} = \begin{cases} 1, & q_i = q_j \\ 0, & q_i \neq q_j \end{cases} \tag{7}$$

The Hamiltonian results in an energy increase whenever neighboring sites have dissimilar orientation states. This energy contribution is attributed to the presence of an interface (i.e., a grain boundary). Therefore, the interaction strength can be viewed as equivalent to the interfacial energy.

While PMC ultimately leads to a minimization of the global free energy through reduction of the interface, it can accept states that lead to energy increases due to its stochastic nature. This is probabilistically expressed by Boltzmann statistics where the transition follows the probability distribution

$$P = \begin{cases} p_0, & \Delta\mathcal{H} \leq 0 \\ p_0 \exp\left(-\frac{\Delta\mathcal{H}}{k_B T}\right), & \Delta\mathcal{H} > 0 \end{cases} \tag{8}$$

where p_0 is the "ground state" probability that a grain will reorient into its neighbor's orientation, $\Delta\mathcal{H}$ is the energy change for the trial configuration, k_B is the

Boltzmann constant, and T is the temperature.

It should be noted that PMC's mathematical formulation has been extensively studied, especially when applied to microstructural evolution kinetics.[14–17] This vast amount of work has shown that the model is able to capture the correct kinetics, topology, and grain size distribution of curvature-driven grain growth for ideal grain growth. Furthermore, its simplicity and easy implementation has made it a popular model when simulating parabolic kinetics.

2.3 PMC Neighborhood Selection

One of the primary features in the PMC model is that grain boundaries are governed by positive energy contributions from unlike neighbors, which simulate interfacial energy (as previously defined). The neighborhood choice itself is an important feature that influences the numerical implementation. For square or cubic lattices, it has been found that the commonly used Von Neumann neighborhood does not correctly reproduce grain growth kinetics, but that the Moore neighborhood does.[23] Thus, nearly all modern PMC model studies use the Moore neighborhood, as shown in Fig. 2. These neighborhood configurations result in 8 and 26 neighbors per lattice site for 2-D and 3-D domains, respectively. Even with the better-performing Moore neighborhood, PMC is known to experience lattice pinning effects at low temperatures. It should be noted that recently, a model by Mason *et al.*[24] has demonstrated reduced lattice artifacts by using a Gaussian-based kernel to define the neighborhood. However, this results in a substantial computational cost increase.

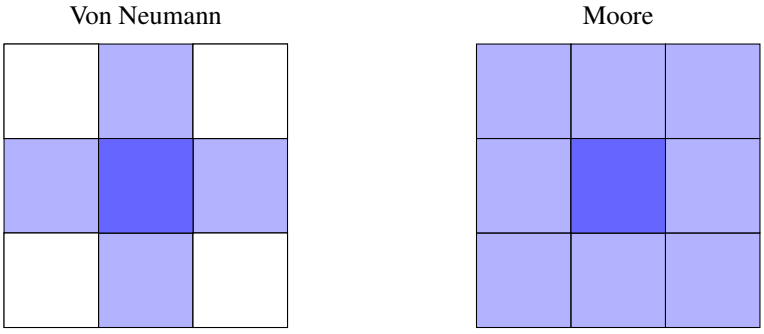

Fig. 2 Neighborhood listing for calculating interfacial properties

2.4 Influence of Grain Boundaries

Low-angle grain boundaries (LAGBs) are very common in naturally formed and processed (under certain conditions) polycrystalline materials resulting in a lower global energy state. LAGBs can be thought of as dislocations arrays, with their properties depending on their orientation. Nonetheless, under far-from-equilibrium processing conditions like severe plastic deformation, materials tend to yield large densities of high-angle grain boundaries.[25,26] The need to understand how processing can influence microstructural evolution highlights the importance of models that can capture a higher-fidelity microstructural description. One of the most common interfacial energy description of LAGBs is given by the RS equation[22]

$$\gamma = \begin{cases} \gamma_0 \theta_r \left(1 - \ln \theta_r\right) & \theta < \theta_m \\ \gamma_0 & \theta \geq \theta_m \end{cases} \tag{9}$$

where γ_0 is related to the shear modulus and Poisson's ratio, and $\theta_r (\equiv \theta/\theta_m)$ is the ratio between the misorientation angle and the cutoff angle (θ_m). The cutoff angle defines the misorientation at which grain boundaries transition from low- to high-angle boundaries. Previous studies have shown that $\theta_m \geq 45^\circ$ lead to slower kinetics[16] and deviations from the expected misorientation angle distribution.[17] The RS theory treats LAGBs as a network of dislocations. This formulation asymptotically converges to the maximum interfacial energy (γ_0) as the misorientation angle approaches the cutoff angle. To model grain interactions in AppPottsRS, Eq. 9 is inserted in Eq. 6 yielding a texture-sensitive Hamiltonian.

As we are considering the likelihood that a grain boundary will migrate leading to grain growth, Eq. 8, the p_0 probability is given by Humphreys' mobility formulation[27]

$$p_0 = \frac{M_{ij}}{M_m} = 1 - \exp\left(-5\left[\frac{\theta}{\theta_m}\right]^4\right) \tag{10}$$

where M_m is the maximum grain boundary mobility.

3. Results

The AppPottsRS implementation into SPPARKS was validated against the well-established literature on PMC. These validation tests include characterization of the code's grain growth kinetics and textural evolution. This section includes the performance tests, and an example of microstructural evolution under thermal gradients.

3.1 Performance

AppPottsRS was benchmarked against other readily available Potts implementation (SPPARKS classes).[19,28] These are the standard PMC (AppPotts), an extension where only neighboring states are sampled as trial reorientations (AppPottsNeigh), and the AppPottsNeighOnly, which also limits sampling to neighboring orientations but also rejects self-similar "reorientations". For the three "native" SPPARKS classes, the total number of permissible orientations (q_N) was set to 128. As a more robust microstructural description is used, there are computational costs associated with the implementation of AppPottsRS. To understand whether the extra computational cost is prohibitive, a series of tests was performed and compared to the highly efficient AppPottsNeighOnly class[20] on the Department of Defense's (DOD's) Topaz SGI ICEX system using a single node (36 cores).[29] Note that these studies focus on testing AppPottsRS's performance as compared to AppPottsNeighOnly since SPPARKS has been thoroughly tested for scalability and performance.[19] The computational costs are shown in Fig. 3, where green bars correspond to cost for various *run times* (fixed domain size) and the blue bars correspond to varying *domain size* (fixed run time). Each `run` was executed three times with different random seeds and the averages were used to determine the corresponding ratios. Due to the preprocessing required by SPPARKS in creating and formatting new variables (angle arrays), loop (main SPPARKS execution) and wall times were considered. These are shown in Fig. 3a and 3b, respectively. A summary for the loop time is shown in Table 1, clearly outlining that AppPottsRS is 5 to 25 times more expensive than AppPottsNeighOnly. Furthermore, the variability in computational expense is regularly larger for AppPottsRS.

However, both loop and wall times show that the AppPottsRS overhead decreases as the simulation run times increases. This is due to the large cost of generating and bookkeeping of single voxel "grain". Hence, as the microstructure evolves and

grains grow, the need to compute the misorientation angle decreases as these have been calculated and stored within the `misos` dictionary. This dictionary (`C++` map) stores the misorientation angle ratio for neighboring grains with q_i and q_j states as $\texttt{misos}(q_i, q_j) = \theta_r$. Also, we see that the expense seems to plateau as the domain size increases. The initial sharp increase is due to the rapidly growing number of randomly oriented grains requiring calculation of the misorientation angle.

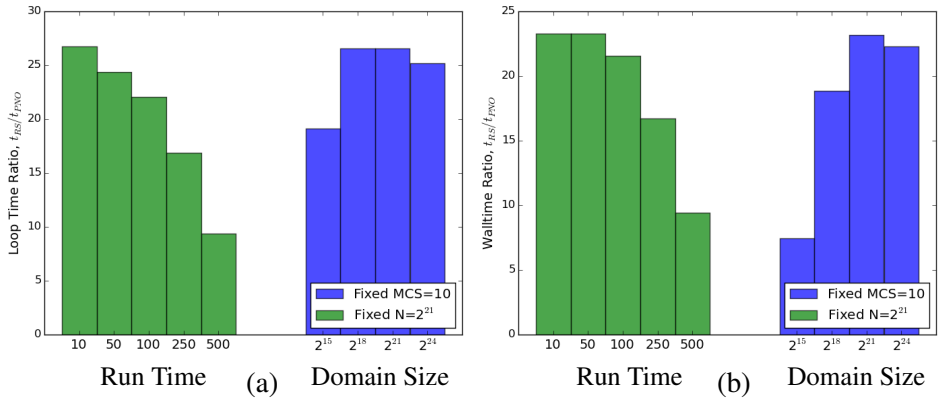

Fig. 3 Relative time expense of AppPottsRS as compared to AppPottsNeighOnly for (a) loop time to evolve the system and (b) wall time to execute the program. Note that the green bars correspond to evolution of a domain with $N = 128 \times 128 \times 128 = 2^{21}$ sites and varying computational times (t_{comp}), while blue bars are for increasing number of sites (N) for a constant t_{comp}

While naturally AppPottsRS will be more expensive, the extra computational demand is affordable with the available infrastructure. The fixed size studies (green bars) suggests that once the computational domain is defined and conditioned, the simulation expense converges to that of AppPottsNeighOnly. Furthermore, these expenses could be decreased by seeding microstructures where each grain has a volume larger than a single voxel (e.g., small grains with a given texture). In fact, this is probably desired as the RS model is not expected to properly capture the physics that lead from a "molten" state (i.e., where each voxel has a unique orientation). Other alternatives to improve efficiency could be a tabulation of mobilities for a predetermined set of grain orientations.

3.2 Grain Growth Kinetics and Size Distribution

All the simulations presented in this section and forward were performed on a local RHEL 7.5 workstation. A `128×128×128` domain is used at a simulation temperature of $k_B T = 0.5$, a cutoff angle of $\theta_m = 25°$, and cubic symmetry. The latter

Table 1 Summary of simulation loop timing test. These tests were performed on a single node (36 processes) on the DOD's Topaz[29]

Run $\{\text{MCS}^{\dagger}, 2^n\}$	App*	Average time, $\bar{t}$ (s)	$\sigma_{\bar{t}}$
$\{10, 15\}$	PNO	0.078683	0.000526
	RS	1.503980	0.012874
$\{10, 18\}$	PNO	0.481683	0.014583
	RS	12.783367	0.124221
$\{10, 21\}$	PNO	4.073537	0.028116
	RS	108.269000	0.938426
$\{10, 24\}$	PNO	37.768400	0.062471
	RS	952.182333	4.215091
$\{50, 21\}$	PNO	13.499833	0.053365
	RS	328.765667	2.982782
$\{100, 21\}$	PNO	24.781767	0.059034
	RS	547.023667	10.097621
$\{250, 21\}$	PNO	58.512400	0.302512
	RS	987.534667	83.196287
$\{500, 21\}$	PNO	114.706667	0.459826
	RS	1077.627333	127.528986

†MCS=Monte Carlo step
*PNO=AppPottsNeighOnly, RS=AppPottsRS

value was chosen to be on the higher range of acceptable values for the cutoff angle, typically $\theta_m \leq 30^{\circ}$. The initial configuration is a random texture where each orientation is defined by

$$q_i = \{2\pi\mathcal{R}_u, \arccos(2\mathcal{R}_v - 1), 2\pi\mathcal{R}_w\} \tag{11}$$

where $\mathcal{R}_j$ is an independent random number uniformly distributed between [0,1). For numerical reasons and compatibility to the SPPARKS framework, each unique set of orientation angles is represented by a single integer value. This means that each voxel in the computational domain is defined by four SPPARKS arrays. A representative resulting microstructure is shown in Fig. 4 at an early, mid-, and late grain growth stages. The top row shows the grain ID/orientation (i.e., each color corresponds to a unique set of Euler angles), while the bottom shows the local energy (outlining the grain boundaries). As the Hamiltonian used for these validations only accounts for interfacial energy (i.e., $U_i = 0$), these show the grain boundaries with brighter boundaries having a higher energy. These images exhibit what appears to be typical parabolic grain growth behavior and topology.

It is well known that the local velocity at which a grain boundary travels is proportional to the interface curvature

$$v = \frac{dr}{dt} \equiv \gamma M \kappa = \frac{\gamma M}{r} = \frac{C}{r} \tag{12}$$

where γ is the interfacial energy, M is the grain boundary mobility, and $\kappa = 1/r$ is the grain boundary curvature. Integrating Eq. 12, we get

$$\int_{R_0}^{R} r dr = \int_{0}^{t} C dt \quad \rightarrow \quad R^2 - R_0^2 = \omega t \tag{13}$$

which is known as the ideal (normal or parabolic) grain growth. More generally, this equation can be written as

$$R^n - R_0^n = \omega t. \tag{14}$$

This theoretical relationship has been proposed and validated by a vast body of computational and experimental work.[30–32] It should be noted that this ideal growth can only be expected in high-purity single phased isotropic systems.[31] Nonetheless, it's a highly studied and vetted approach that has been found to be applicable to a wide range of microstructural evolution conditions.

To confirm that AppPottsRS does follow the expected growth kinetics, the grain growth curve and size distribution were plotted in Fig. 5. The simulation was run to $t_{\text{comp}} \sim 100$ (i.e., 2600 MCS)

$$t_{\text{comp}} = \text{MCS} \cdot \Delta t \tag{15}$$

where Δt is class specific and MCS is defined as a *computational sweep* where each site (on average) has attempted an orientation change. This computational time was chosen because the small number of grains present at this stage, which leads to poor statistics. The analytic parabolic growth curve is shown, Fig. 5a, which is in good agreement with the simulated data (coefficient of determination, $R^2 = 0.99$). Note that here the grain growth exponent has been fixed to $n = 2$ to assess AppPottsRS's ability to predict parabolic grain growth. Figure 5b shows the normalized grain area/size distribution. The area was calculated under the assumption that grains topologically approximate spheres and that the grain volume is given by the number

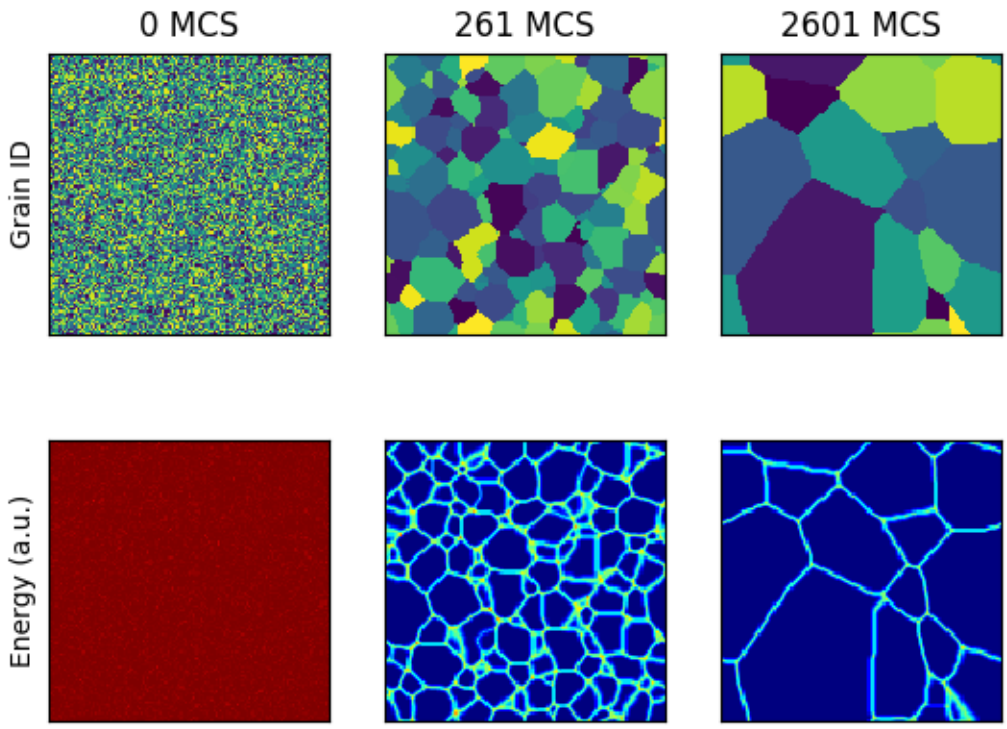

Fig. 4 Simulated microstructural evolution using the AppPottsRS class at three different times showing the (top) grain orientation and (bottom) local energy. These are the `XY` plane at the center of the 3-D simulation

of sites (voxels) comprising the grain cluster

$$A = \pi R^2 = \pi \sqrt[3]{\left(\frac{3 \cdot n_{vx}}{4\pi}\right)^2} \tag{16}$$

where n_{vx} is the number of voxels in the grain cluster. As expected,[17] it agrees with isotropic untextured materials where most grain are about the same size but with a distinctive negative skewness (toward smaller grains). Furthermore, it shows that the size distribution is time invariant as long as enough grains are available to calculate reliable statistics.

As previously mentioned, AppPottsRS was benchmarked against other SPPARKS's Potts-based algorithms. Figure 6 shows the final simulation state for AppPottsRS and the other three AppPotts variants available within SPPARKS. Notice that these correspond to $t_{\text{comp}} = 100$, which scales with the MCS. For AppPotts, the time

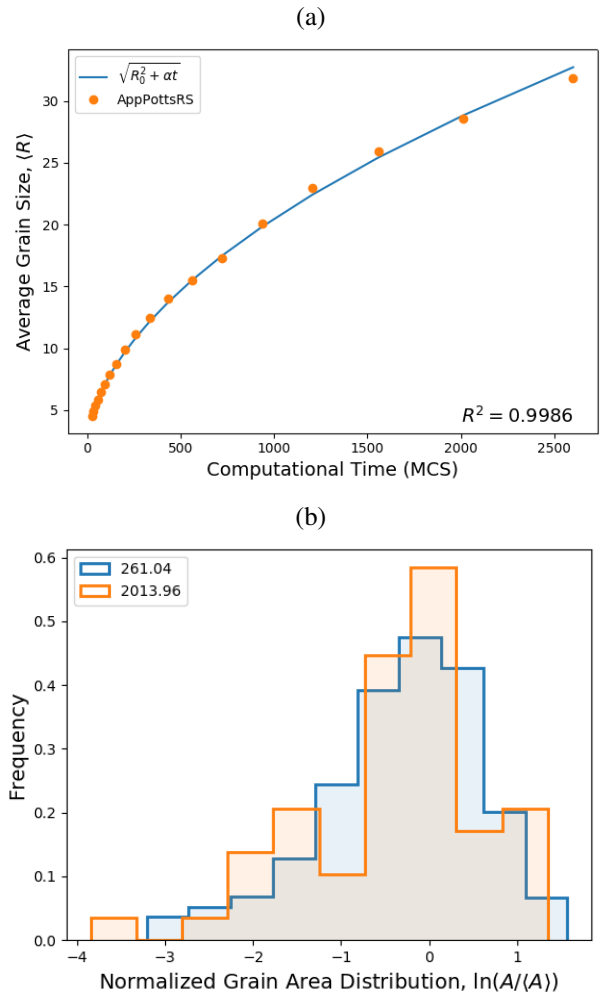

Fig. 5 Grain growth kinetics as simulated by AppPottsRS in a randomly textured polycrystal: (a) grain growth curve with analytical fit and (b) grain area distribution for two computational times

step between MCS is $\Delta t = 1/q_N = 1/128$, while the other implementations use $\Delta t = 1/\max(n_{nei}) = 1/26$. This means that for the same computational time, AppPotts has performed many more sweeps, or each voxel has attempted to reorient more times. Visually inspecting Fig. 5 shows that AppPotts and AppPottsNeigh are in agreement, while AppPottsRS and AppPottsNeighOnly correlate to each other. The main difference arises from the fact that AppPottsRS and AppPottsNeighOnly only allow sampling of unlike neighbor states, while AppPotts and AppPottsNeigh equally weight each allowable state. Therefore, the probability of rejecting a trial increases for the AppPotts and -Neigh algorithms.

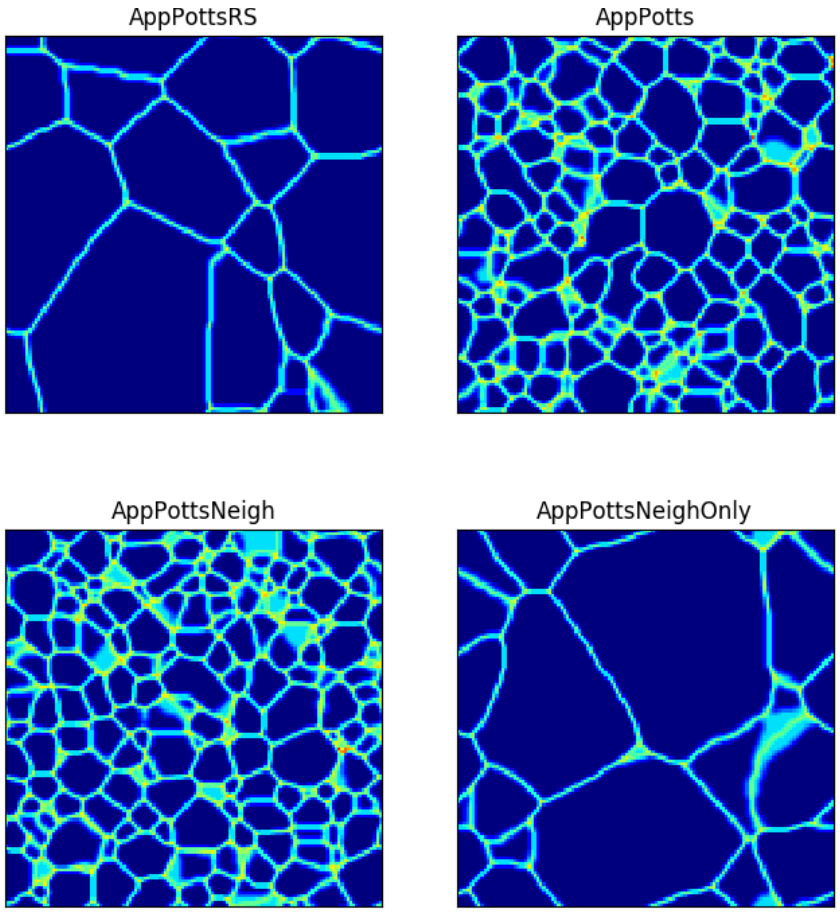

Fig. 6 Representative microstructure at equivalent computational times ($t_{\mathbf{comp}} = 100$) for the different AppPotts classes. Plots show local energy, which outline grain boundaries. These are the `XY` plane at the center of the 3-D simulation

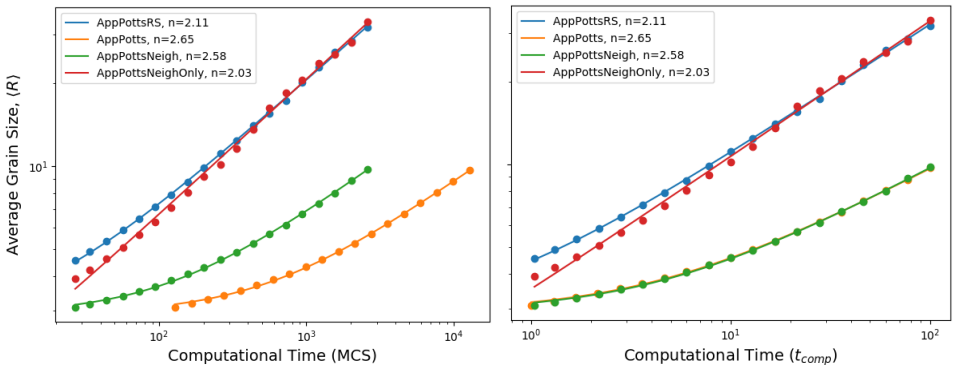

Fig. 7 Grain growth curves for the multiple SPPARKS AppPotts classes. The two figures plot the same grain growth simulations under different time variables: (a) MCS and (b) t_{comp}

These differences between the AppPotts classes can be better appreciated from plotting the grain growth curves, in Fig. 7. Here, the simulated data are fit to the generic grain growth form (Eq. 14) to determine how the growth exponents compare. As shown in the legend, while the growth exponentials are in the right neighborhood, these are not precisely the expected parabolic growth values ($n \equiv 2$). There are multiple reasons for this discrepancy. Firstly, these were performed on a relatively small domain due to computational efficiency reasons. While larger runs can be executed, for the purposes of validation the domain used was deemed acceptable. Secondly, most work in the literature outlines the assumption that $R \gg R_0$, leading to Eq. 14 being rewritten as $R^n \equiv \alpha t$. Lastly, it should be pointed out that these average sizes were determined by filtering out any grain cluster below a given threshold (12 voxels). Using thresholds going from 0 to 26 resulted in similar trends. However, as smaller grains are filtered out the growth exponent approaches the parabolic value ($n \rightarrow 2$).

It should be noted that by transforming the time-scale to computational time, AppPotts and AppPottsNeigh fall right on top of each other. This can be explained by understanding that the time-step is related to the probability of sampling an allowable spin state, wherein AppPotts scales by q_N and AppPottsNeigh by the number of neighbors. All of this said, it is shown that AppPottsRS follows AppPottsNeighOnly's kinetics as both of these classes reject self-similar orientations.

The last validation test was to measure the grain boundary misorientation angle distribution (MDF), as shown in Fig. 8. The distribution of misorientation angles was

determined by accounting for each grain pair present in the simulation (i.e., number grain boundaries instantiations). It is expected that the Mackenzie distribution function[33,34] be obtained as these tests simulated evolution of an initially random textured cubic material. As can be seen from Fig. 8 there is good agreement between the numerical and expected distributions. As shown, this distribution seems to be fairly temperature independent. It should be noted that steady-state misorientation angle distribution is mainly influenced by thermodynamics (Hamiltonian), as opposed to kinetics (mobility).[17]

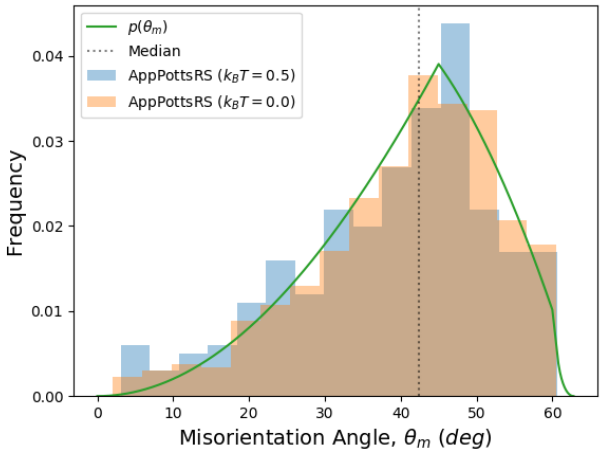

Fig. 8 Misorientation angle distribution for initially random textured materials. The $p(\theta)$ curve corresponds to the piecewise function developed by Mackenzie[33]

3.3 Evolution under Temperature Gradient

To test the AppPottsRS class under more useful conditions, microstructural evolution simulations under temperature gradients were performed. These temperature gradients followed linear and Gaussian-based profiles in the normal direction (ND, or Z axis). These gradients enable nonuniform probabilities of accepting a trial configuration (grain reorientation) whenever the reorientation leads to an increases in energy ($\Delta\mathcal{H} > 0$). Furthermore, the gradients lead to local grain boundary mobilities as these depend on temperature. This dependence was introduced by changing the mobility term shown in Eq. 10

$$M_{ij}(T) = M_{ij} \cdot \exp\left(-\frac{Q}{k_B T}\right) \tag{17}$$

where Q is the grain boundary motion activation energy. Figure 9 shows the com-

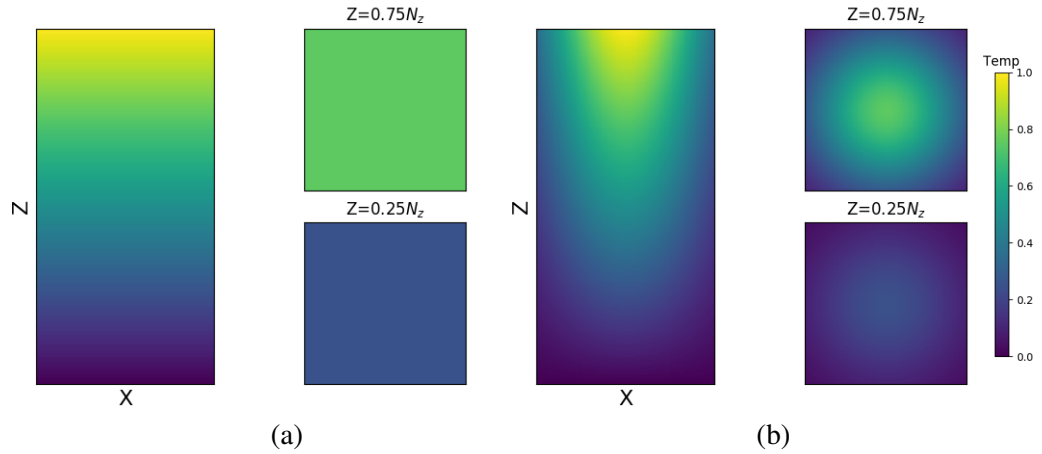

Fig. 9 Inverse temperature ($1/k_BT$) profiles used to simulate microstructural evolution under a) linear and b) Gaussian-based temperature gradients

putational temperature (k_BT) profiles, where the brighter region (yellow) has the highest local temperature ($k_BT|_{z=N_z} \sim 1.0$). In turn, the probability of boundary migration is given by

$$p_0 = \left\{1 - \exp\left(-5\left[\frac{\theta}{\theta_m}\right]^4\right)\right\} \cdot \exp\left(-\frac{Q}{k_BT}\right) \tag{18}$$

where the likelihood of a grain boundary advancing is influence by both textural and thermal conditions. The linear profile corresponds to a uniform heat source at the top surface of the "sample", while the Gaussian profile corresponds to a point source at the center of the top surface ($0.5\{N_x, N_y, 2N_z\}$). To properly capture and clearly showcase the effect of thermal gradients, the computational domain used was elongated in the ND (i.e., $100 \times 100 \times 200$ voxels were used). To remain consistent with previous sections, a cutoff angle of $\theta_m = 25°$, and cubic symmetry were used.

For visualization purposes, the local energy was thresholded to higher values ($\mathcal{H}_i > 5$ a.u.) to clearly delineate grain boundaries, and in turn the microstructure. Visualizing the microstructure in this way provides an easy approach to interpret the influence of the temperature gradient. The resulting 3-D grain boundaries structure is shown in Fig. 10 for the linear temperature gradient where the temperature is highest at the top surface. As expected, microstructural evolution depends on the local temperature as it influences the velocity at which grain boundaries travel (mobility). Hence, average grain sizes are larger towards the top where temperatures are higher, and boundaries faster. It should be noted that the bottom regions showing

a dense red volume arises from the fact that grains are unable to grow due to the low temperature ($M_{ij}|_{T\sim 0} \rightarrow 0$). Therefore, the microstructure is made up of single voxel-sized grains, leading to very high local interfacial energies. An interesting aspect of the Gaussian profile is its nonconstant temperature nature on the XY planes. Figure 11 shows this dependence by slicing the XZ plane at three different locations along the transverse direction (Y axis). This showcases the important of carefully characterizing and comparing simulations with locally dependent properties, (e.g., microstructural evolution under laser welding).[35,36]

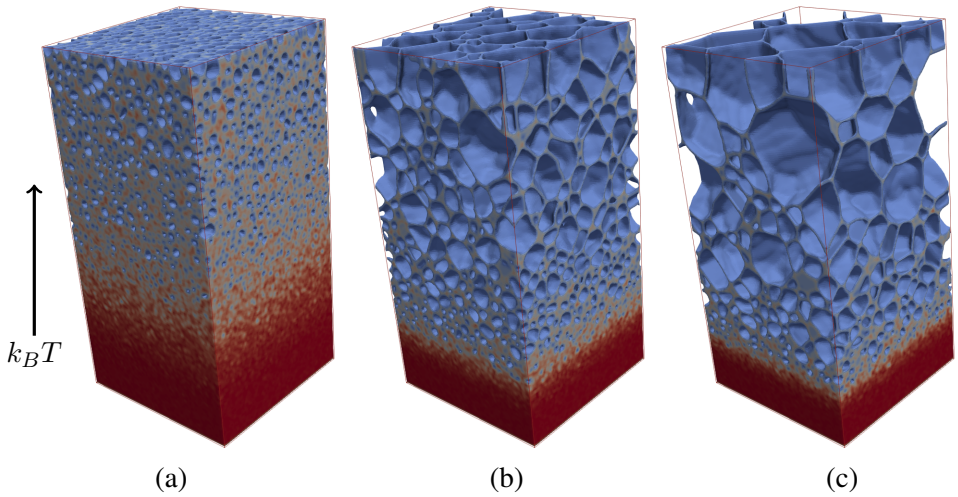

Fig. 10 Microstructural evolution under a linear thermal gradient at three different times: a) 73, b) 935, and c) 2601 MCS

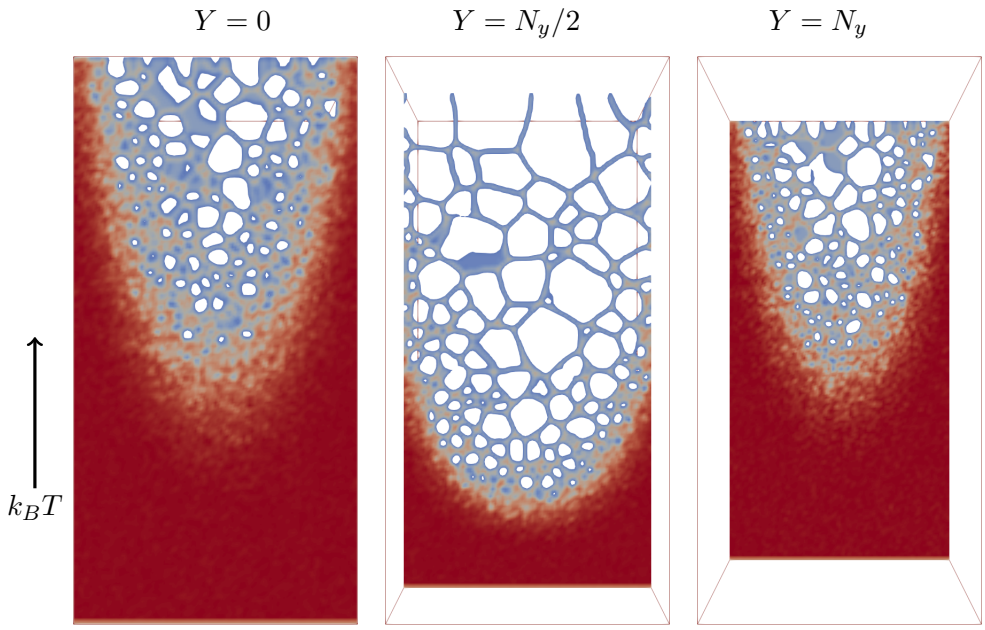

Fig. 11 Gaussian-based temperature profiles at the boundary surfaces ($Y = \{0, N_y\}$) and center ($Y = N_y/2$) of the computational domain at two times

Lastly, the grain boundary structures evolution for the linear and Gaussian temperature profiles at different times are shown in Fig. 12. These slices were taken at $Y = N_y/2$ to properly compare between the two cases (i.e., the planes containing the maximum temperature gradient). As before, it is shown that higher temperature regions lead to larger grains as grain boundaries are more mobile. An interesting feature is that tracking the grain boundary migration along the ND for the two profiles looks very similar around the center-line. This clearly delineates how local processing conditions have a controlling influence on the microstructural evolution.

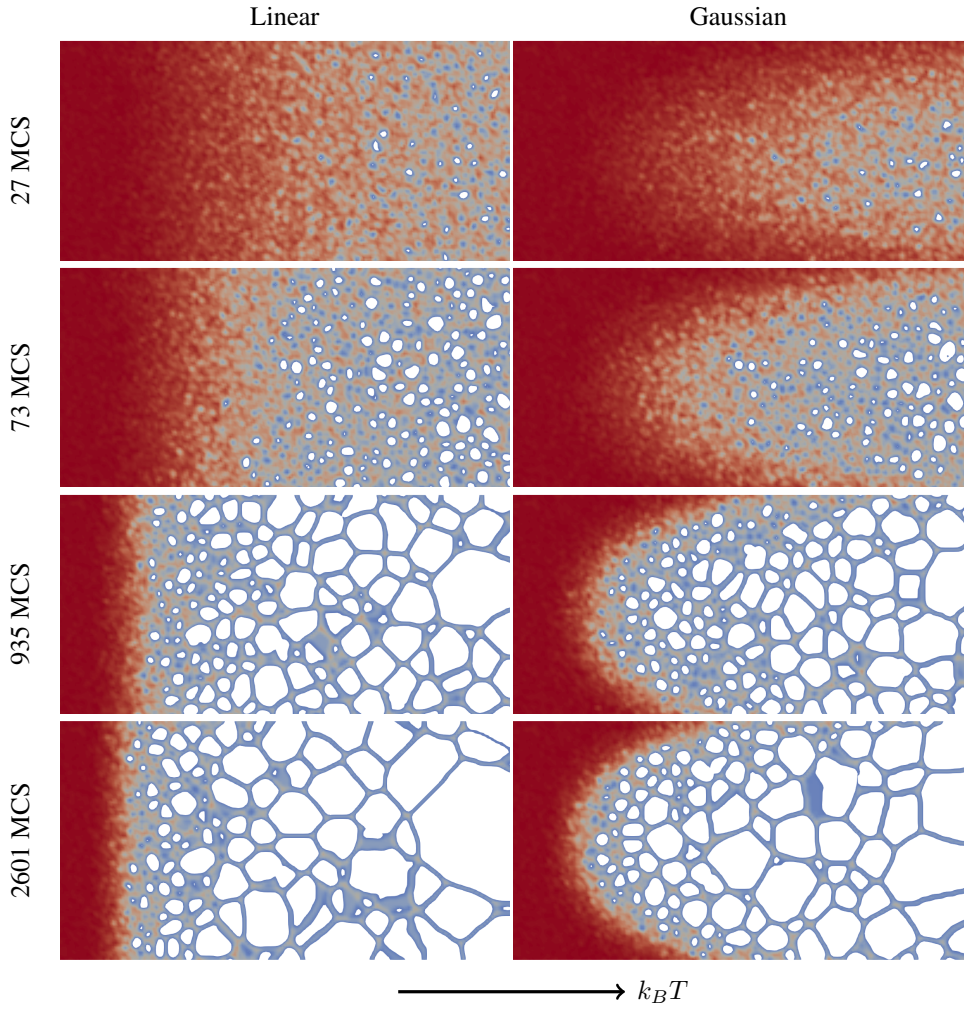

Fig. 12 Comparison between linear and Gaussian-based temperature distributions

4. Conclusion

The AppPottsRS class, based on Read–Shockley's interfacial model, is presented to simulate microstructural evolution of anisotropic materials. The implementation was developed as a `C++` class compatible with the SPPARKS framework, enabling large simulations through multiprocessing computations. The implementation was based on SPPARKS' AppPottsNeighOnly algorithm. A time study was performed to understand the computational overhead introduced by AppPottsRS over the traditional AppPottsNeighOnly algorithm. It is shown that while there is a noticeable expense, this quickly decreases as the simulation run time increases. This is due to the initial expense of defining the orientation angles and corresponding grain boundary misorientation angles. It is also shown that the AppPottsRS class results in larger computational cost variabilities.

To validate the code, a series of well-understood and well-studied simulated microstructural properties were analyzed. These included grain growth exponent, average grain size distribution, and grain boundary misorientation distributions. It was shown that AppPottsRS is able to reproduce expected features like parabolic grain growth. The grain size distribution was shown to be time invariant and to be negatively skewed. Further, it was shown how the class compares to the other three AppPotts classes available from the SPPARKS package. As is to be expected, the newly developed class best agrees with AppPottsNeighOnly as they implement similar rejection algorithms. It is shown that all four implementations are able to capture parabolic-like grain growth. When considering the distribution of grain boundary angles, the AppPottsRS was able to reproduce the Mackenzie distribution. Moreover, it is shown that this distribution is temperature invariant.

Lastly, two temperature-gradient profiles were used to model microstructural evolution under locally varying temperatures. These local variations lead to changes in the grain boundary mobilities, which result in graded microstructures. An interesting observation was that tracking the location of the "high local energy" surface (about the centerline) resulted in similar evolution for both profiles. This shows the importance of these local environments.

5. References

1. Hall E. The deformation and ageing of mild steel: III discussion of results. Proc Physical Soc B. 1951;64(9):747.

2. Petch N. The cleavage strength of polycrystals. J Iron Steel Inst London. 1953;173:25–28.

3. Mishra R, Balasubramaniam R. Effect of nanocrystalline grain size on the electrochemical and corrosion behavior of nickel. Corr Sci. 2004;46(12):3019–3029.

4. Martirena H, Burfoot J. Grain-size effects on properties of some ferroelectric ceramics. J Physics C: Sol State Phys. 1974;7(17):3182.

5. Lu L, Shen Y, Chen X, Qian L, Lu K. Ultrahigh strength and high electrical conductivity in copper. Science. 2004;304(5669):422–426.

6. Zinkle SJ, Snead LL. Designing radiation resistance in materials for fusion energy. Ann Rev Mat Res. 2014;44:241–267.

7. Senkov O, Senkova S, Woodward C, Miracle D. Low-density, refractory multi-principal element alloys of the Cr–Nb–Ti–V–Zr system: microstructure and phase analysis. Acta Materialia. 2013;61(5):1545–1557.

8. Kocks UF, Tomé CN, Wenk HR, Beaudoin AJ. Texture and anisotropy: preferred orientations in polycrystals and their effect on materials properties. Cambridge (UK): Cambridge University Press; 2000.

9. Zhao HK, Chan T, Merriman B, Osher S. A variational level set approach to multiphase motion. J Comp Phys. 1996;127(1):179–195.

10. Chen LQ. Phase-field models for microstructure evolution. Ann Rev Mat Res. 2002;32(1):113–140.

11. Potts RB. Some generalized order-disorder transformations. Math Proc Cambridge Phil Soc. 1952;48:106–109.

12. Ising E. Beitrag zur Theorie des Ferromagnetismus. Zeitschrift für Physik. 1925;31(1):253–258.

13. Onsager L. Crystal statistics. I. A two-dimensional model with an order-disorder transition. Physical Rev. 1944;65(3-4):117.

14. Anderson M, Srolovitz D, Grest G, Sahni P. Computer simulation of grain growth-I. Kinetics. Acta Metallurgica. 1984;32(5):783–791.

15. Srolovitz D, Anderson MP, Sahni PS, Grest GS. Computer simulation of grain growth-II. Grain size distribution, topology, and local dynamics. Acta Metallurgica. 1984;32(5):793–802.

16. Grest G, Srolovitz D, Anderson M. Computer simulation of grain growth-IV. Anisotropic grain boundary energies. Acta Metallurgica. 1985;33(3):509–520.

17. Holm EA, Hassold GN, Miodownik MA. On misorientation distribution evolution during anisotropic grain growth. Acta Materialia. 2001;49(15):2981–2991.

18. Wu FY. The Potts model. Rev Mod Phys. 1982;54(1):235.

19. Plimpton S, Battaile C, Chandross M, Holm L, Thompson A, Tikare V, Wagner G, Webb E, Zhou X, Garcia-Cardona C, Slepoy A. Crossing the mesoscale no-man's land via parallel kinetic Monte Carlo. Sandia National Laboratories; 2009. Report No.: SAND2009-6226.

20. Sandia National Laboratories. SPPARKS documentation: app_style potts. [accessed 2018 Jul 26]. http://spparks.sandia.gov/doc/app_potts.html.

21. Hernández-Rivera E. AppPottsRS: a Read–Shockley class for SPPARKS. Aberdeen Proving Ground (MD): Army Research Laboratory (US); 2018 Sep. Report No.: ARL-TN-0913.

22. Read WT, Shockley W. Dislocation models of crystal grain boundaries. Physical Rev. 1950;78(3):275.

23. Holm EA, Glazier JA, Srolovitz DJ, Grest GS. Effects of lattice anisotropy and temperature on domain growth in the two-dimensional Potts model. Physical Rev A. 1991;43(6):2662.

24. Mason J, Lind J, Li S, Reed B, Kumar M. Kinetics and anisotropy of the Monte Carlo model of grain growth. Acta Materialia. 2015;82:155–166.

25. Iwahashi Y, Horita Z, Nemoto M, Langdon T. An investigation of microstructural evolution during equal-channel angular pressing. Acta Materialia. 1997;45(11):4733–4741.

26. Valiev R, Alexandrov I, Zhu Y, Lowe T. Paradox of strength and ductility in metals processed by severe plastic deformation. J Mat Res. 2002;17(1):5–8.

27. Humphreys F. A unified theory of recovery, recrystallization and grain growth, based on the stability and growth of cellular microstructures–I. The basic model. Acta Materialia. 1997;45(10):4231–4240.

28. SPPARKS documentation. Sandia National Laboratories. [accessed 2018 Jul 26]. http://spparks.sandia.gov/.

29. Hardware. Army Engineer Research and Development Center (US): DOD Supercomputing Resource Center. [accessed 2018 Jul 02]. https://www.erdc.hpc.mil/hardware/index.html.

30. Mullins W, Vinals J. Self-similarity and growth kinetics driven by surface free energy reduction. Acta Metallurgica. 1989;37(4):991–997.

31. Atkinson H. Overview no. 65: theories of normal grain growth in pure single phase systems. Acta Metallurgica. 1988;36(3):469–491.

32. Burke J, Turnbull D. Recrystallization and grain growth. Prog Met Phys. 1952;3:220–292.

33. Mackenzie J. Second paper on statistics associated with the random disorientation of cubes. Biometrika. 1958;45(1-2):229–240.

34. Handscomb D. On the random disorientation of two cubes. Can J Math. 1958;10:85–88.

35. Rodgers TM, Mitchell JA, Tikare V. A Monte Carlo model for 3D grain evolution during welding. Model Sim Mat Sci Eng. 2017;25(6):064006.

36. SPPARKS documentation: app_style potts_weld. Sandia National Laboratories. [accessed 2018 Jul 26]. https://spparks.sandia.gov/doc/app_potts_weld.html.

List of Symbols, Abbreviations, and Acronyms

2-D	2-dimensional
3-D	3-dimensional
DOD	Department of Defense
ID	identification
LAGB	low-angle grain boundaries
MCS	Monte Carlo step
ND	normal direction
PMC	Potts Monte Carlo
RS	Read–Shockley
SPPARKS	Stochastic Parallel PARticle Kinetic Simulator

1 (PDF) DEFENSE TECHNICAL INFORMATION CTR
DTIC OCA

2 (PDF) DIR ARL
IMAL HAR
RECORDS MGMT
RDRL DCL
TECH LIB

1 (PDF) GOVT PRINTG OFC
A MALHOTRA

3 (PDF) SANDIA NATIONAL LABORATORIES
S PLIMPTON
T RODGERS
V TIKARE

3 (PDF) AIR FORCE RESEARCH LABORATORY
A GERLT
E PAYTON
A PILCHAK

52 (PDF) DIR USARL
RDRL-CIH-C
J CRONE
J KNAP
RDRL WML B
B RICE
D TAYLOR
RDRL WML H
B SCHUSTER
RDRL WMM
J BEATTY
J MCCAULEY
RDRL WMM B
B AKSOYLU
C FOUNTZOULAS
A GAYNOR
G GAZONAS
E HERNANDEZ
D HOPKINS
J LIGDA
B LOVE
D MAGAGNOSC
J PITTARI
B POWERS
T SANO
T WALTER
R WILDMAN
RDRL WMM D
D GALLES
K HART
F KELLOGG
C KUBE
B MCWILLIAMS
C MOCK
RDRL WMM E
K BEHLER
V BLAIR
R BRENNAN
S COLEMAN
A DIGIOVANNI
M GOLT
M GUZIEWSKI
J LASALVIA
RDRL WMM F
K DARLING
R DOWDING
S FUDGER
A GIRI
P GOINS
C HAINES
B HORNBUCKLE
K LIMMER
H MURDOCH

RDRL WMM G
J ANDZELM
B RINDERSPACHER
T SIRK
RDRL WMP C
R BECKER
J CLAYTON
J LLOYD
A TONGE